J. Radiat. Res., 50, 513–519 (2009)

Regular Paper

Effects of Interfractional Anatomical Changes on Water-Equivalent Pathlength in Charged-Particle Radiotherapy of Lung Cancer

Shinichiro MORI*, Hsiao-Ming LU, John A. WOLFGANG, Noah C. CHOI and George T. Y. CHEN

Charged-particle/Four-dimensional/Lung cancer/Lung density/Radiotherapy planning/Beam range variation/Tumor shrinkage.

Intrafractional motion and interfractional changes affect the accuracy of the delivered dose in radiotherapy, particularly in charged-particle radiotherapy. Most recent studies are focused on intrafractional motion (respiratory motion). Here, we report a quantitative simulation analysis of the effects of interfractional changes on water-equivalent pathlength (WEL) in charged-particle lung therapy. Serial four-dimensional (4D) CT scans were performed under free breathing conditions; the time span between the first and second 4DCT scans was five weeks. We quantified WEL changes between the first and second CT scans due to interfractional changes (tumor shrinkage and tissue density changes) and compared the particle-beam-stopping point between the serial 4DCT scans with use of the same initial bolus. Both tumor-shrinkage and lung-density changes were observed in a single patient over the course of therapy. The lung density decreased by approximately 0.1 g/cm^3 between the first and second-CT scans, resulting in a 1.5 cm WEL changes. Tumor shrinkage resulted in approximately 3 cm WEL changes. If the same initial bolus and plan were used through the treatment course, an unexpected significant beam overshoot would occur by interfractional changes due to tumor shrinkage and lung density variation.

INTRODUCTION

Dose conformation requires accurate knowledge of the geometry of the target. In the treatment of thorax and abdomen, recent developmental efforts in dose conformation have been focused on mitigating the effects of respiratory motion by using respiratory-correlated or tracking irradiating methods.[1–4] Clinical implementation of these techniques have been reported.[1,5] Another source of intrafractional motion, cardiac motion, can also affect treatment accuracy.[6]

Charged-particle beams are particularly sensitive to intrafractional motion because of their finite beam range. The water-equivalent pathlength (WEL), can be calculated by weighting the physical pathlength with the HU (Hounsfield unit) value per pixel.[7] Temporal variations in the WEL along the same ray lead to variation of the geometric depth of penetration (overshoot or undershoot relative to the nominal beam stopping point).

*Corresponding author: Phone: +81-43-251-2111,
Fax: +81-43-284-0198,
E-mail: shinshin@nirs.go.jp
Massachusetts General Hospital, Harvard Medical School, Department of Radiation Oncology
doi:10.1269/jrr.09032

Other sources of beam range perturbations include those resulting from interfractional changes of tumor size, tumor shape, tissue thickness, etc. Tumor shrinkage has been observed over the course of treatment, and its effect on dose distribution has been reported.[8–10] A quantitative analysis of WEL changes due to interfractional changes during a treatment course is the purpose of this paper.

MATERIALS AND METHODS

Patient and data acquisition

The patient signed an informed consent for CT scanning and treatment when she agreed to be treated with photons. The subject of our simulation study was a female patient aged 77 years with non-small-cell lung cancer (IIIA) (cT2N2M0). The tumor (5.7 cm (left-right: LR) × 5.1 cm (anterior-posterior: AP) cm × 5.2 cm (superior-inferior: SI)) was located in the right middle lobe. In addition, chemotherapy was administered. A weight loss of 9.1 kg was recorded over a period of five weeks. The prescribed dose to the planning target volume (PTV) was 43.2 Gy in 24 fractions, followed by a dose of 19.8 Gy to a smaller volume in 11 fractions, for a total dose of 63 Gy delivered by an 8-field IMRT (intensity modulated radiotherapy).

Two CT scan data are used here for assessment of inter-

fractional changes if charged-particle beams were to be used. The first treatment-planning CT scan was performed under free breathing conditions with a 4-slice CT scanner (LightSpeed Qx/i, General Electric Medical Systems, Waukesha, WI) in 4DCT acquisition mode.[11] Patient respiration was monitored by a Real-Time Position Management (RPM) Respiratory Gating System (Varian Medical Systems, Palo Alto, CA). Five weeks after the first CT scan, a second 4D CT scan (second CT scan) was done. A slice collimation of 4 × 2.5 mm was used for both CT scans.

Data analysis

We calculated the changes between the first and second CT scans of the following quantities: (i) the gross tumor volume (GTV), (ii) the tumor center-of-mass motion, (iii) WEL to a specific plane, (iv) regional lung density, and (v) proton beam dose distribution. Image registration was performed by aligning the two 4DCT scans by registration of the bony anatomy at the peak exhalation because respiratory signal is more reproducible than that at other phases. Each respiratory cycle was subdivided into 10 phases (from T0% to T90%), with peak inhalation and peak exhalation defined at T0% and T50%, respectively by using RPM signal. The GTV was contoured manually on axial slices of both first and second CT scan images.

GTV center of mass was calculated by averaging points on the GTV counter lines as a function of a respiratory phase.

In the WEL analysis, the rationale of this metrics is to obtain an estimate of the beam range variations. The calculation region was defined by two planes encompassing the tissues between the entrance surface of the body and the plane tangent to the most distal point of the internal target volume (ITV). The same plane positions were chosen for the second CT scan. The WEL calculation was performed along the beam direction. A WEL change (ΔWEL) was also calculated by subtraction of the WEL of the second CT scan from that of the first CT scan at the same respiratory phase.

A lung density map was calculated for each scan to analyze lung density changes. The lung was first segmented from other anatomic structures by threshold edge detection.[12] A two-dimensional (2D) convolution filter (Gaussian filter)[13] was applied to the 2D AP image in order to smooth noise (3 pixels × 3 pixels). A lung density image was then generated by calculation of the average density, ρ, along the BEV (beam's eye view) direction by using the following equation;

$$\rho = \frac{HU_{air} - HU_{lung}}{HU_{air}} \quad [\mathrm{g/cm^3}],$$

where HU_{lung} and HU_{air} are the average HU (Hounsfield unit) numbers in the lung and air, respectively. We evaluated the lung density variation as a function of respiratory phase by defining a 2-cm-diameter ROI on the upper left and right lung regions in the first and second CT scans.

A bolus was designed to irradiate a moving target in the respiratory gated phase interval as follows: an internal target volume (ITV) was defined for respiratory-gated radiotherapy (RGRT) using the T40%–T60% phase interval (gated phase) in the planning 4DCT scan data.[14] The charged-particle beam with this bolus nominally stops at the distal edge of the gated ITV. Next, this bolus was applied to both first and second CT scans at the exhalation respiratory phase (T50%). A two-field proton dose distribution was calculated for beams at 180° and 300° gantry angles (IEC convention), using a pencil-beam algorithm.[15] These beam angles were selected from the ipsilateral rather than contralateral side of lung and to minimize excessive dose to heart. The PTV included an 8-mm margin around the ITV.

RESULTS

GTV center-of-mass trajectory

The center-of-mass trajectories for the first and second CT scans are shown in Fig. 1. Peak exhalation (T50%) and inhalation (T0%) loci are indicated by solid circles. The solid lines correspond to the gating window (T40–60%). The center-of-mass displacement was 3.5 mm (AP: 1.6 mm, LR: 2.6 mm, SI: 1.7 mm) for the first CT scan and 3.3 mm (AP: 2.3 mm, LR: 1.1 mm, SI: 2.1 mm) for the second CT scan. The center-of-mass trajectory and the difference between the two CT scans were relatively small. Although the peak exhalation positions of the first CT and second CT scans are close, the tumor trajectories differ.

GTV volume changes

Axial images of the first CT and second CT scans at exhale at the same cranio-caudal position are shown in Fig.

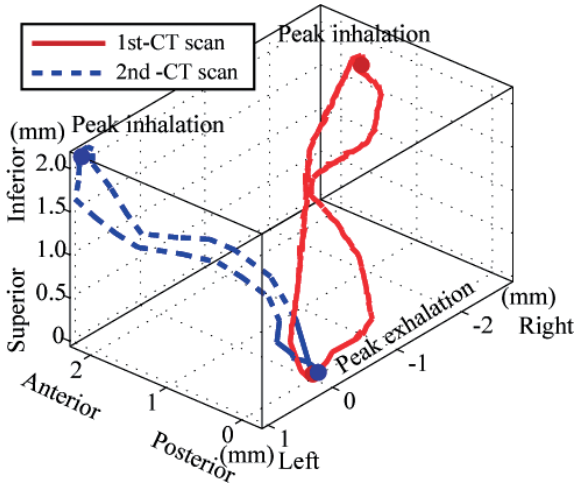

Fig. 1. Tumor center-of-mass trajectory for first and second CT scans in 3D trajectory. The solid lines correspond to the gating window (T40–60%).

2. The tumor shape in the second CT scan shows asymmetric shrinkage compared with that for the first CT scan.

The mean gross tumor volume from all respiratory phases was 115.2 cm^3 (s.d. 1.2 cm^3) in the first CT scan and 39.2 cm^3 (s.d. 1.7 cm^3) in the second CT scan (Fig. 2b). There were no significant variations in volume as a function of respiratory phase for either scan.

WEL change

The WEL change map quantifies the differences in WEL

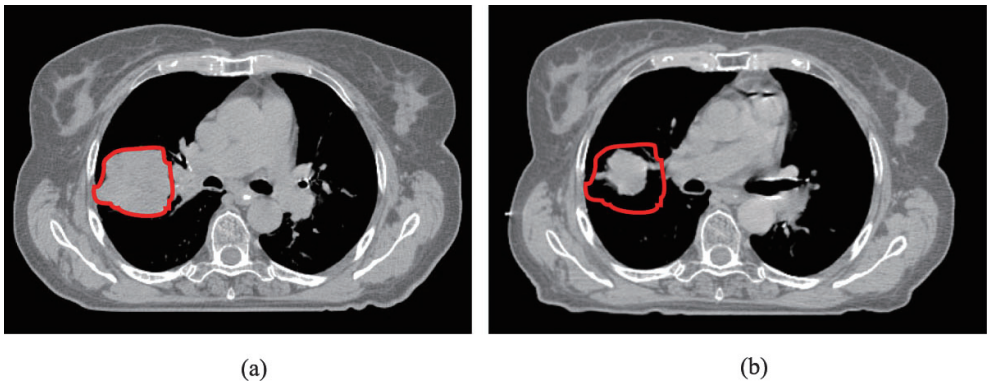

Fig. 2. Axial images at peak exhalation (T50%). (a) First CT scan. (b) Second CT scan. The red contour represents the GTV at time of first CT scan.

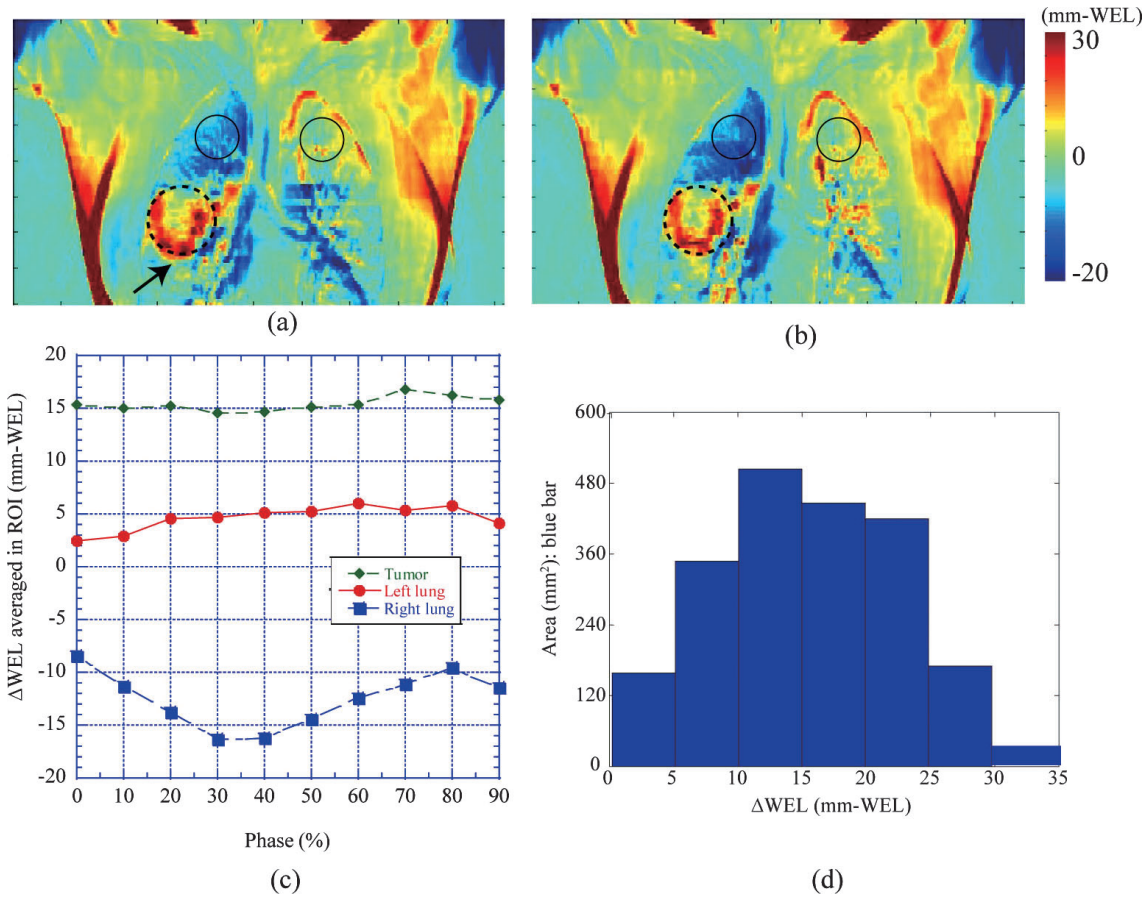

Fig. 3. WEL change (ΔWEL) map at (a) peak inhalation (T0%) and (b) peak exhalation (T50%). (c) ΔWEL in ROIs for the left upper lung, right upper lung (solid circles in Figs. 3a and 3b) and above the tumor (dotted circles in Figs. 3a and 3b). (d) Histogram of ΔWEL (left axis) on the tumor at peak exhalation (T50%).

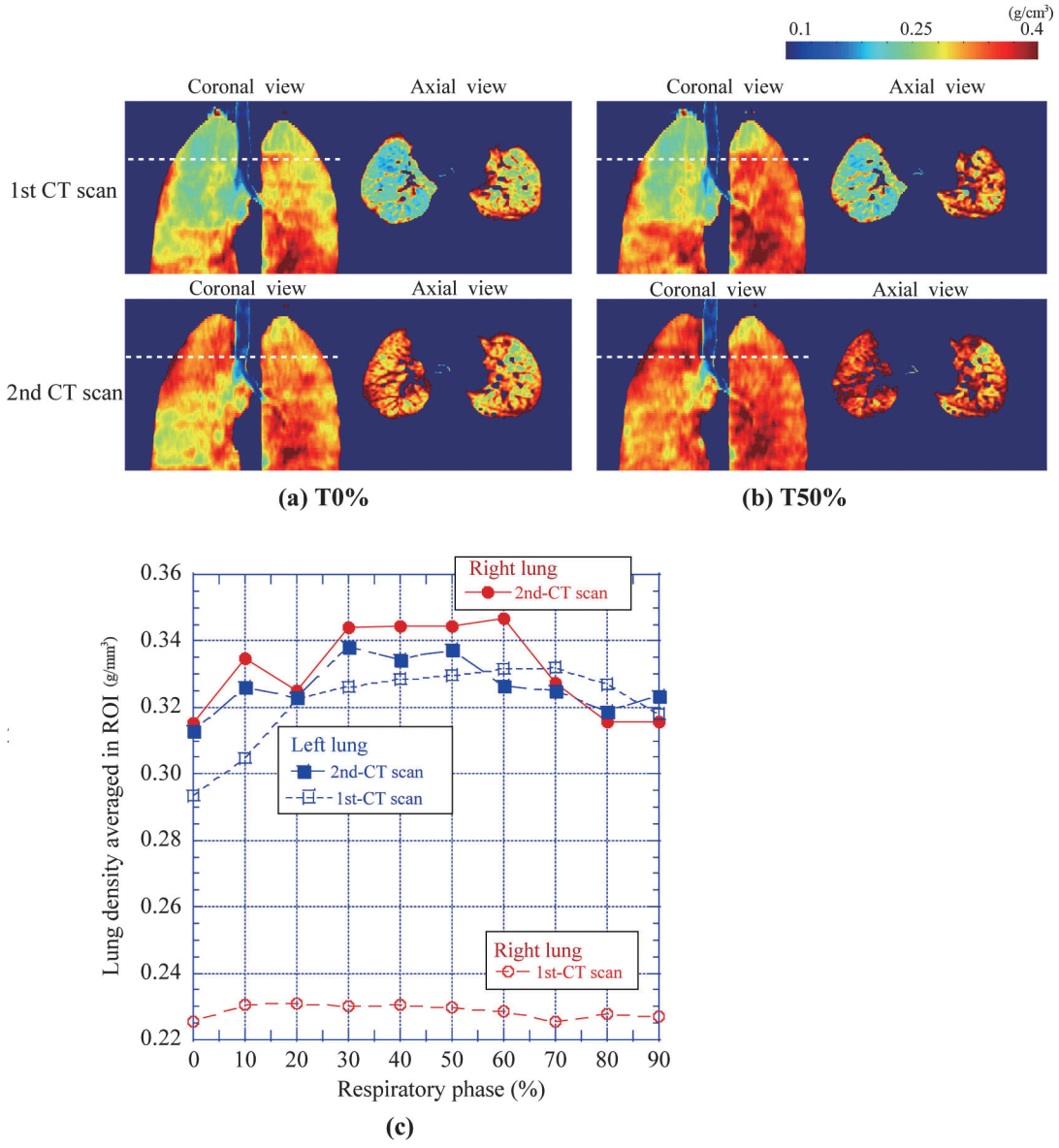

Fig. 4. Lung density maps at two respiratory phases (a) Peak inhalation (T0%). (b) Peak exhalation (T50%). Dotted lines show axial plane location. (c) Average lung density within ROI for first and second CT scans. ROIs were defined on upper left and right lungs.

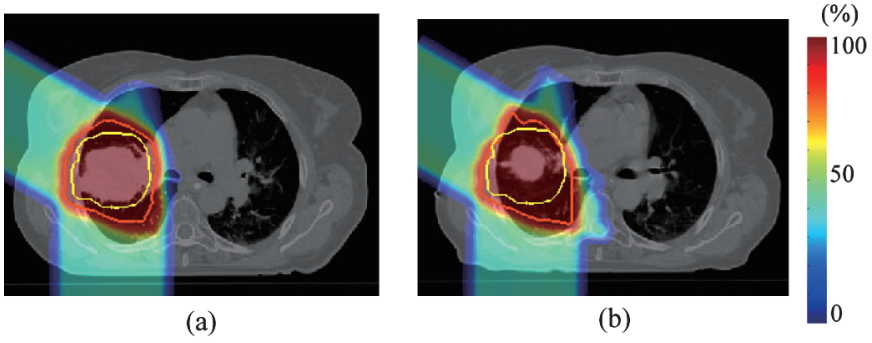

Fig. 5. Proton beam dose distributions. A bolus, designed to cover moving target during gated treatment (T40–60%), is applied to (a) first CT scan and (b) second CT scan at peak exhalation phase (T50%). The beam angle was set to 180° and 300°. Yellow lines demarcate the PTV for the planning CT. Red lines show 95% dose line.

between two CT scans. If there were no changes in WEL, the change maps would show no structure. However, several regions of the WEL change map show significant changes (Figs. 3a and 3b). These change maps indicate that the WEL from the entrance surface to a well defined anatomic plane have changed from the first CT scan to the second scan. Such changes arise because of changes in tissue size or shape, or density changes in the tissues transited.

Consider Fig. 3a; this change map is calculated by first calculating the WEL map for both scans 1 and 2 from the AP direction (to a specified plane). The change map is calculated by subtracting the second scan WEL map from the first (in a mode similar to a subtraction angiogram). Figure 3a is calculated at a respiratory phase of maximum inhale, while Fig. 3b shows the change map at exhale. The external contours and outlines of the lungs are approximately symmetric, and provide an indication that the alignment of the two CT scans is reasonable. However, specific regions of the WEL change map show significant positive / negative WEL changes. A WEL change (< 15 mm) was observed at the superior edge of the left lung because of inexact registration of this organ. A WEL change of greater than 20 mm was observed at the edge of the breast because of weight loss (and / or breast positioning). The periphery of the heart showed a negative WEL change (blue region) resulting from cardiac motion. There was a rim of positive WEL change near the inferior portion of the tumor due to shrinkage (marked as arrow in Fig. 3a). The lung tissue above the tumor showed negative WEL change, as indicated by the blue region (marked as circles in Figs. 3a and 3b).

To evaluate WEL changes at each respiratory phase, we defined three circular regions of interest (ROIs), two in the two upper lungs and one over the tumor. The average ΔWEL of these ROIs is shown in Fig. 3c. WEL change in the left lung over the entire respiratory cycle were less than 6 mm (mean: 4.6 mm, s.d. 1.2 mm) and were nearly constant throughout the respiratory cycle. The ΔWEL in the right-lung ROI (above the tumor) exhibited a substantial change of approximately –16 mm (mean: –12.5 mm, s.d. 2.7 mm) over all phases. This beam range change is a function of the respiratory phase. The tumor ROI showed a WEL of less than 17 mm (mean: 15.4 mm, s.d. 0.7 mm) averaged over all respiratory phases; this was attributed to tumor shrinkage. The maximum ΔWEL was 34.7 mm (pixel value) (see the black arrows in Fig. 3a).

The tumor ROI included a region where the tumor had shrunk and been replaced by lower-density lung tissue. Because the tumor center-of-mass displacement was small, the ΔWEL image at peak exhalation (T50%) was selected, and the ROI over the tumor region was plotted in the histogram in Fig. 3d. About 640 mm^2 of this ROI showed a ΔWEL of greater than 20 mm, and 1090 mm^2 of the ROI showed a ΔWEL of greater than 15 mm.

Lung density changes

Lung density maps for the first and second CT scans are shown in Figs. 4a and 4b. The left-lung densities were unchanged in both CT scans; however, a lower lung density was observed in the right upper lung region in the first CT scan.

The lung density in the contralateral lung showed that left lung density in both CT scans is essentially unchanged; 0.32 g/cm^3 and 0.33 g/cm^3 averaged over all respiratory phases. Furthermore, these lung densities decreased slightly at inhalation because of the expanding lung volume. In the right lung above the tumor, however, the lung density in the ROI changed from 0.23 g/cm^3 (first CT scan) to 0.33 g/cm^3 (second CT scan) averaged over all respiratory phases, corresponding to a density change of approximately 0.1 g/cm^3.

Dose distribution

Figure 5 shows the proton beam dose distributions (T50%) for treatment beams at 180º and 300º. Because the first bolus was designed based on the first planning scan, the charged-particle beam stopped as planned (Fig. 5a). However, use of the first bolus on the second CT scan would have resulted in significant beam overshoot because of tumor shrinkage and weight loss (Fig. 5b). At the 300º angle, the overshoot reached the spinal cord.

DISCUSSION

We have reported on WEL variations due to interfractional changes as observed in serial 4DCT scans. The key findings of this investigation are tumor shrinkage and lung density changes resulted in approximately 3 cm and 1.5 cm WEL variation, respectively. These WEL variations are dependent on patient characteristics such as tumor size or tumor position. Although only a single patient was evaluated, our results indicate that using a first bolus and a first treatment plan throughout a charged-particle therapy course can be problematic. Furthermore, the results of our study are one of the first steps toward a better understanding of how to reduce uncertainties caused by interfractional changes in charged-particle therapy of the lung.

RGRT is currently in clinical use in a number of centers. With this technique, the tumor is irradiated at its most reproducible position during the respiratory cycle, usually at peak exhalation. With RGRT, beam range fluctuations due to respiration are reduced in comparison to free breathing radiotherapy. Significant beam overshoot was observed in this patient even though RGRT was used, because of tumor shrinkage.

The tumor volume in the patient decreased by 76 cm^3 between the two 4DCT scans. The volume occupied by the tumor after shrinkage was replaced by lung tissue, with a density change from 0.95 g/cm^3 (tumor) to 0.33 g/cm^3 (lung). This density change results in beam over-penetration

that is twice as great as the pathlength of tissue replaced along the beam axis. Because the bolus is designed to cover the PTV based on the first CT scan, the charged-particle beam with this bolus correctly stops along the distal edge of the PTV in early fractions. However, application of this first bolus would result in beam overshoot in late fractions due to tumor shrinkage. The overshoot causes undesired dose to normal tissues.

The other source of beam range variation in this patient is a lung density change, resulting in a 1.5 cm WEL change. Figure 4 shows that the density of the left lung in the first CT scan varied as expected over the respiratory cycle; the same variation of density as a function of respiratory phase was observed in the second CT scan, indicating normal lung function. The resulting ΔWEL image of the left lung was nearly constant, indicating little relative change over an interval of several weeks. In contrast, in the upper right lung, the density did not vary during respiration, indicating limited air exchange. However, in the second scan, the right lung density did change during breathing in a manner similar to that in the left lung (see Fig. 4c). Possible clinical explanations of the increase in density are 1) subclinical pneumonia or 2) increased perfusion due to tumor shrinkage. This unexpected lung density change can potentially decrease the accuracy of irradiation, and suggests the need for frequent monitoring of density changes during the course of treatment.

Other sources of beam range uncertainty include 1) tumor trajectory variations between the first and second CT scans and 2) weight loss. Britton *et al*. reported such variations by analyzing the tumor center-of-mass trajectory seen in weekly serial 4DCT data.[16] If the first bolus and aperture design does not cover the beam range of tumor motion due to respiration, even with RGRT, the dosimetric coverage can be compromised. In this study, the tumor trajectory did not affect beam overshoot because of minimal tumor motion.

Recently, there has been interest and implementation of hypo-fractionated carbon ion beam or proton beam treatments for lung cancer.[17,18] In hypofractionated carbon ion beam treatment, issues such as tumor shrinkage or lung density changes, may not be as great a concern because the treatments are given over just a few days. The variation of center of mass trajectory and WEL fluctuation from one fraction to another may still be a concern, and additional studies are needed.

CONCLUSION

Multiple factors in intrafractional motion and interfractional change can affect the beam range in charged-particle therapy. Interfractional changes can result in significant beam overshoot if the first bolus is applied over the entire course of therapy. Replanning[19] and redesigning of the bolus to account for interfractional changes must be considered in addition to intrafractional motion mitigation to deliver treatment beams with greater accuracy.

ACKNOWLEDGEMENT

The authors thank Dr. Michael Goitein for helpful discussions. We would like to express our appreciation to Dr. Michael Folkert for his assistance.

REFERENCES

1. Ohara, K., Okumura, T., Akisada, M., Inada, T., Mori, T., Yokota, H., *et al*. (1989) Irradiation synchronized with respiration gate. Int. J. Radiat. Oncol. Biol. Phys. **17**(4): 853–857.
2. Inada, T., Tsuji, H., Hayakawa, Y., Maruhashi, A. and Tsujii, H. (1992) [Proton irradiation synchronized with respiratory cycle]. Nippon Igaku Hoshasen Gakkai Zasshi **52**(8): 1161–1167.
3. Berbeco, R., Jiang, S. B., Sharp, G. C., Chen, G. T. Y., Mostafavi, H. and Shirato, H. (2004) Integrated radiotherapy imaging system (IRIS): design considerations of tumour tracking with linac gantry-mounted diagnostic x-ray systems with flat-panel detectors. Physics in Medicine and Biology **49**: 243–255.
4. Shirato, H., Shimizu, S., Kitamura, K. and Onimaru, R., (2007) Organ motion in image-guided radiotherapy: lessons from real-time tumor-tracking radiotherapy. International Journal of Clinical Oncology **12**(1): 8–16.
5. Giraud, P., Yorke, E., Ford, E. C., Wagman, R., Mageras, G. S., Amols, H. *et al*. (2006) Reduction of organ motion in lung tumors with respiratory gating. Lung Cancer **51**(1): 41–51.
6. Jones, B. and Akine, Y. (2006) Dose distribution to the mediastinum and heart. Br. J. Radiol. **79**(941): 448.
7. Kanematsu, N., Matsufuji, N., Kohno, R., Minohara, S. and Kanai, T. (2003) A CT calibration method based on the polybinary tissue model for radiotherapy treatment planning. Phys. Med. Biol. **48**(8): 1053–1064.
8. Hansen, E. K., Bucci, M. K., Quivey, J. M., Weinberg, V. and Xia, P. (2006) Repeat CT imaging and replanning during the course of IMRT for head-and-neck cancer. Int. J. Radiat. Oncol. Biol. Phys. **64**(2): 355–362.
9. Kupelian, P. A., Ramsey, C., Meeks, S. L., Willoughby, T. R., Forbes, A., Wagner, T. H. *et al*. (2005) Serial megavoltage CT imaging during external beam radiotherapy for non-small-cell lung cancer: observations on tumor regression during treatment. Int. J. Radiat. Oncol. Biol. Phys. **63**(4): 1024–1028.
10. Willoughby, T. R., Forbes, A. R., Buchholz, D., Langen, K. M., Wagner, T. H., Zeidan, O. A. *et al*. (2006) Evaluation of an infrared camera and X-ray system using implanted fiducials in patients with lung tumors for gated radiation therapy. Int. J. Radiat. Oncol. Biol. Phys. **66**(2): 568–575.
11. Vedam, S. S., Keall, P. J., Kini, V. R., Mostafavi, H., Shukla, H. P. and Mohan, R. (2003) Acquiring a four-dimensional computed tomography dataset using an external respiratory signal. Phys. Med. Biol. **48**(1): 45–62.
12. Yang, F., Wan, S. and Chang, Y. (2005) Improved Method for Gradient-Threshold Edge Detector Based on HVS. Computational Intelligence and Security **3801**: 1051–1056.

13. Bracewell, R. (1999) "Convolution" and "Two-Dimensional Convolution." Ch. 3 in The Fourier Transform and Its Applications, 3rd ed. 25–50 and 243–244.
14. Mori, S., Wolfgang, J., Lu, H. M., Schneider, R., Choi, N. C. and Chen, G. T. (2008) Quantitative assessment of range fluctuations in charged particle lung irradiation. Int. J. Radiat. Oncol. Biol. Phys. **70**(1): 253–261.
15. Petti, P. L. (1992) Differential-pencil-beam dose calculations for charged particles. Med. Phys. **19**(1): 137–149.
16. Britton, K. R,, Starkschall, G., Tucker, S. L., Pan, T., Nelson, C., Chang, J. Y., *et al*. (2007) Assessment of gross tumor volume regression and motion changes during radiotherapy for non-small-cell lung cancer as measured by four-dimensional computed tomography. Int. J. Radiat. Oncol. Biol. Phys. **68**(4): 1036–1046.
17. Miyamoto, T., Baba, M., Yamamoto, N., Koto, M., Sugawara, T., Yashiro, T. *et al*. (2007) Curative treatment of Stage I non-small-cell lung cancer with carbon ion beams using a hypofractionated regimen. Int. J. Radiat. Oncol. Biol. Phys. **67**(3): 750–758.
18. Bush, D. A., Slater, J. D., Shin, B. B., Cheek, G., Miller, D. W. and Slater, J. M. (2004) Hypofractionated proton beam radiotherapy for stage I lung cancer. Chest **126**(4): 1198–1203.
19. Kato, S., Ohno, T., Tsujii, H., Nakano, T., Mizoe, J. E., Kamada, T. *et al*. (2006) Dose escalation study of carbon ion radiotherapy for locally advanced carcinoma of the uterine cervix. Int J Radiat Oncol Biol Phys **65**(2): 388–397.

Received on March 27, 2009
Revision received on June 8, 2009
Accepted on July 13, 2009